PERGAMON

Journal of Structural Geology 21 (1999) 585–596

JOURNAL OF STRUCTURAL GEOLOGY

Mechanical controls on fault geometry

Stephen J. Martel

University of Hawaii, Department of Geology and Geophysics, Honolulu, HI 96822, USA

Received 14 July 1998; accepted 22 February 1999

Abstract

Faults inevitably become non-planar because of how they grow and how they are affected during slip by mechanical heterogeneities inherent in the earth. Some faults acquire a non-planar geometry because of non-uniform tectonic deformation or because they grow by the linkage of originally discontinuous structures. However, even faults that are originally planar are unlikely to remain so. Elastic analyses show that as a fault slips, it rotates with the surrounding rock. It rotates uniformly and remains planar if: (a) the shear stress drop along the fault is uniform, (b) the rock surrounding the fault is uniform and isotropic, and (c) the far-field stress state is uniform. Variation in stress drop or in fault strength, heterogeneity in host-rock stiffness, and interaction with other faults cause non-uniform rotation along a fault that slips, and the fault geometry deforms. Mechanical and geometrical heterogeneities are inherent in the earth, so all natural faults will tend to become non-planar to some degree as they slip, even if they were initially planar. Information on fault shape can illuminate the mechanics of faulting, and, in conjunction with slip data, help locate contacts between rock bodies of different elastic moduli. In uniform isotropic rocks, fault curvature is proportional to the rate at which the stress drop varies as a function of position along a fault, whereas the slip profile reflects a weighted average of the stress drop.

1. Introduction

The geometry of a fault provides a fundamental control on its mechanical behavior and reflects the processes by which the fault grew. Although faults commonly are idealized as planar, most in fact are not. Faults at all scales contain échelon segments, have bends, or are curved or warped to some degree (e.g. Sylvester, 1988). Perhaps the most famous example is the 'Big Bend' of the San Andreas fault, a plate boundary several hundred kilometers long. Wallace and Morris (1986) discussed several examples of non-planar faults exposed in three dimensions within mines in Idaho; these faults extend for several kilometers or more. Non-planar fault geometries also appear at the scale of outcrops (e.g. Fig. 1) for faults with trace lengths of less than 100 m (e.g. Segall and Pollard, 1983; Martel et al., 1988; Martel, 1990; Swanson, 1990; Bürgmann and Pollard, 1994). This paper discusses why faults assume non-planar geometries and shows how curved fault geometries can be analyzed.

Non-planar fault geometries control a variety of important geologic processes. Earthquakes commonly nucleate or are arrested at bends or steps along faults (Schwartz and Coppersmith, 1986). Sedimentary basins commonly form at bends along faults, ranging in area from sag ponds of several hundred square meters to depressions of several hundred square kilometers (Aydin and Nur, 1982; Sylvester, 1988). Clusters of secondary fractures commonly form at bends or steps (e.g. Woodcock and Fischer, 1986). These fracture clusters probably account for why fault steps are sites for fluid flow as manifest by ore bodies and geothermal fields (Sibson, 1987). A more complete explanation of how faults develop non-planar geometries thus should be of both practical and academic interest.

Non-planar fault geometries arise for a variety of reasons. Some faults have deformed in response to either regional (i.e. tectonic) or local deformation, such as that associated with a nearby intrusion. This deformation need not be associated with fault slip. It can

E-mail address: martel@soest.hawaii.edu (S.J. Martel)

0191-8141/99/$ - see front matter
PII: S0191-8141(99)00054-1

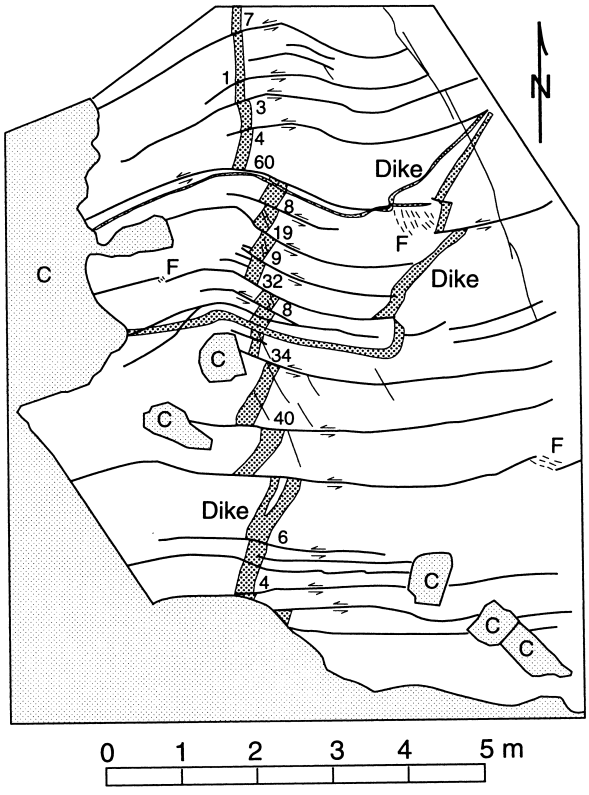

Fig. 1. Map of kinked left lateral faults, aplitic dikes (dark shading), and NNW-striking joints from an outcrop near the Hilgard Branch of Bear Creek in the Mount Abbot quadrangle, California. Numerals denote left-lateral separation in cm of dike margin. C = covered area. F = foliation. The bearing to Mount Hilgard is 69° and the distance is 3.4 km.

occur either in the period when the fault slips or after slip has ceased. A fault could also have its geometry changed by being offset by another fault. Other geometry changes arise solely as a result of heterogeneous mechanical conditions along a fault; these geometry changes are the focus here.

Some faults become non-planar as they grow by linkage of pre-existing, discontinuous, non-coplanar structures (Segall and Pollard, 1980, 1983; Rispoli, 1981; Martel et al., 1988; Cruikshank et al., 1991; Bürgmann and Pollard, 1994; Cruikshank and Aydin, 1994; Willemse et al., 1997). Whether faults generally grow by linkage or instead propagate as shear fractures is a matter of some debate (e.g. Petit and Barquins, 1988). Shear fractures that appear to propagate in-plane have been produced in laboratory experiments (e.g. Cox and Scholz, 1988a,b). Scholz and his co-workers (e.g. Cowie and Scholz, 1992a,b; Scholz et al., 1993; Vermilye and Scholz, 1998) have presented analyses consistent with faults propagating as planar shear fractures. The analyses here focus on whether a fault could become non-planar even if it did not grow by the linkage of non-coplanar structures.

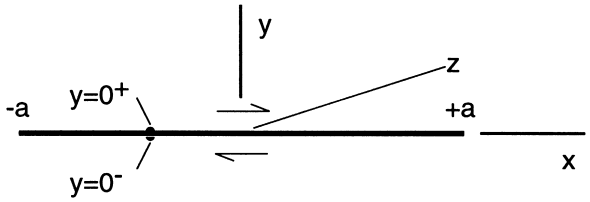

Fig. 2. Two-dimensional mode II fault and reference frame. The y-axis is perpendicular to the fault. The x-axis parallels the short, in-plane dimension of the fault. The z-axis axis parallels the infinite dimension of the fault (i.e. it is out of the page). Positions near the fault are in terms of the complex number $z = x + iy$.

Analytical and numerical solutions from elasticity theory illustrate how fault geometry is distorted during slip. These solutions are based on infinitesimal strain theory and apply most rigorously to the initial distortion of fault geometry. Non-elastic finite deformation associated with faulting (e.g. Bürgmann and Pollard, 1994) cannot be quantified well with these analyses. Nonetheless, the effects identified might be amplified as non-elastic deformation builds. The analyses show that mechanical and geometrical heterogeneities inevitably cause faults to become distorted as they slip. The analyses here parallel and complement those of Bürgmann et al. (1994) in their study of effects of mechanical and geometric factors on fault slip distributions.

An example of kinked small faults from the Mount Abbot quadrangle (Fig. 1) allows tests of the theoretical predictions. The first analysis serves as a reference; it shows how fault geometry is affected by slip in a uniform material along a fault of uniform strength (or stress drop) where the stress field far from the fault also is uniform. Examinations of non-uniform stress drop, fault interaction, and heterogeneity in host rock stiffness follow. Each of these three sections discusses how various mechanical factors jointly affect slip distribution and fault geometry.

2. Kinked faults of the Mount Abbot quadrangle

Monoclinal kink bands defined by kinked left-lateral faults (e.g. Fig. 1) occur in several places in the Mount Abbot quadrangle (Segall and Pollard, 1983; Davies and Pollard, 1986; Martel et al., 1988). These kinks have nearly vertical fold axes and develop where numerous short faults parallel a few much longer faults. The sense of kinking is conjugate to that of the slip across the faults (Fig. 1). Almost all the kinks identified to date occur near or along dikes that strike at nearly right angles to the faults. The localized nature of the kinks and their small size indicate that they form as a result of localized heterogeneities, not regional deformation gradients.

3. Elementary models

The model of an isolated two-dimensional fault in a homogeneous, isotropic, isothermal, linear elastic material serves as a reference of comparison for more complicated fault models. The term 'fault' is used rather than 'model fault' henceforth for the sake of brevity. The fault is perpendicular to the y-axis and extends an infinite direction along the z-axis (Fig. 2). The fault is represented by a cut of length $2a$ that extends along the x-axis from $x=-a$ to $x=+a$ (Fig. 2 inset). The regional stress field far from the fault is uniform and permits slip parallel to the x-axis. Displacements are confined to the x,y-plane (i.e. plane strain applies).

Two methods are used here for calculating displacements along a fault. Analytical solutions use Westergaard stress functions (Westergaard, 1939; Tada et al., 1973; Bürgmann et al., 1994; Martel, 1997). Along the fault, where y goes to zero, the displacements depend only on the stress function $\bar{Z}$. The component of displacement perpendicular to the fault is u_y, and that parallel to the fault is u_x. According to Tada et al. (1973), displacements at the fault walls are:

$$u_y(y=0)=\frac{-(1-2\nu)}{2G}\mathrm{Re}\,\bar{Z}, \tag{1a}$$

$$u_x(y=0^+)=\frac{(1-\nu)}{G}\mathrm{Im}\,\bar{Z}, \tag{1b}$$

where G is the shear modulus, ν is Poisson's ratio, and Re and Im refer to the respective real and imaginary parts of the stress function $\bar{Z}$. The other method used for calculating displacements is boundary element analysis (e.g. Crouch and Starfield, 1983), a numerical method. The boundary element solutions are used for cases not amenable to treatment with stress functions. They also are used to check analytical solutions of Tada et al. (1973) because some of those solutions are in error.

This manuscript focuses on the distortion of fault geometry. Displacement of a fault differs entirely from the relative displacement (i.e. slip) *across* a fault or the displacement u_x at the fault walls. Slip across a fault, Δu_x, equals $u_x(y=0^+)-u_x(y=0^-)$. For the symmetric cases considered here $\Delta u_x=2u_x(y=0^+)$. On a fault, $u_x(y=0)$ is zero; slip does not cause a fault to lengthen or shorten in the x-direction. In contrast, $u_y(y=0)$ generally will not be zero along a fault; this displacement component dictates how fault geometry is distorted out of plane.

3.1. Uniform stress drop along a two-dimensional fault

In a uniform, isotropic material under uniform far-field stresses, the deformation also is uniform. Hence, a passive marker that was planar prior to deformation will remain planar afterwards. In contrast, deformation associated with fault slip generally is not uniform and can result in changes in fault shape. Displacements associated with fault slip can be calculated directly from the shear stress drop $\Delta\tau$ associated with slip, where $\Delta\tau=\tau^{\infty}-\tau^{\mathrm{fault}}$ (Pollard and Segall, 1987). The term τ^{fault} is the shear stress, or frictional strength, on the fault after sliding, and τ^{∞} is the far-field shear stress parallel to the fault. If τ^{fault} drops below τ^{∞}, then the fault will slip. The stress drop $\Delta\tau$ is positive here for right-lateral slip. The Westergaard stress function $\bar{Z}$ for a uniform stress drop is a function of position z (Tada et al., 1973):

$$\bar{Z}(z)=\Delta\tau\left\{\sqrt{z^2-a^2}-z\right\}. \tag{2}$$

The term z equals $x+\mathrm{i}y$ (Fig. 2). Along the fault, z

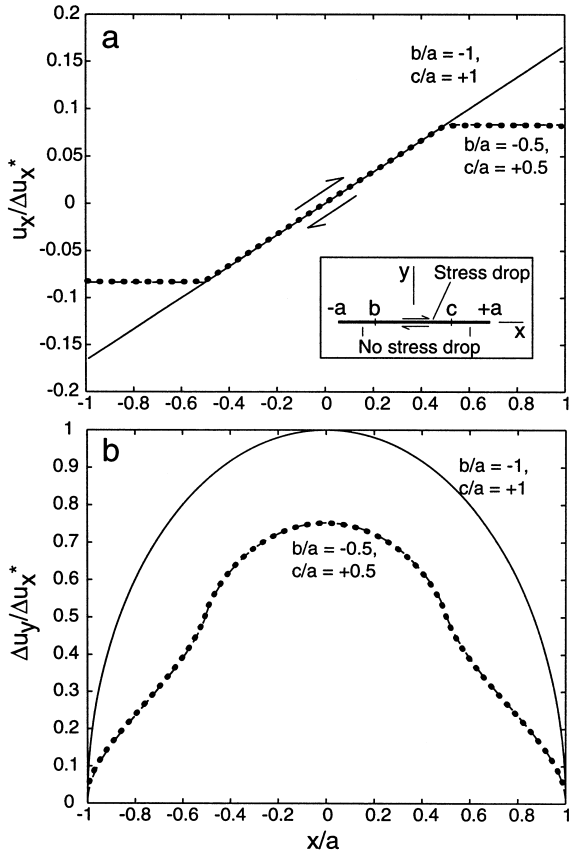

Fig. 3. Profiles of normalized (a) fault-normal displacement ($u_y/\Delta u_x^*$) and (b) slip ($\Delta u_x/\Delta u_x^*$) vs position (x/a) along a fault with a stepped shear stress distribution (dashed line). The shear stress drop along the interval $b<x<c$ is $\Delta\tau$, and the shear stress drop along the remainder of the fault is zero. Here and in all subsequent graphs, the profiles are normalized by the maximum value of slip for an isolated fault with a uniform stress drop (Δu_x^*), lines mark analytical solutions, solid lines mark the reference case of a uniform stress drop, dots or stars mark numerical solutions, and Poisson's ratio equals 0.25.

equals x and is purely real, and $\sqrt{(x^2 - a^2)}$ is purely imaginary. As a result, $\mathrm{Re}\,\bar{Z} = (-\Delta\tau)(x)$ and $\mathrm{Im}\,\bar{Z} = \Delta\tau\sqrt{(a^2 - x^2)}$. Eqs. (1a) and (1b) thus yield the following expressions for u_y and u_x at $y = 0^+$:

$$u_y = \frac{\Delta\tau(1-2\nu)}{2G}x, \tag{3a}$$

$$u_x = \frac{\Delta\tau(1-\nu)}{G}\sqrt{a^2 - x^2}. \tag{3b}$$

The maximum slip, Δu_x^*, occurs at $x = 0$. For a fault of half-length a in a uniform isotropic material, $\Delta u_x^* = 2(1-\nu)(\Delta\tau/G)a$; this value is used as a scaling factor in the figures of this paper. Eq. (3a) shows that u_y scales with distance along the x-axis from the origin. The magnitude of u_y is largest near the fault ends and smallest at the middle, reversing sign across the fault center (Fig. 3a, solid line). The fault thus rotates from its orientation prior to slip. A right-lateral fault rotates counterclockwise, and a left-lateral fault rotates clockwise. The rotation angle ω is:

$$\omega = \tan^{-1}\left(\frac{\mathrm{d}u_y}{\mathrm{d}x}\right). \tag{4}$$

Substituting Eq. (3a) into Eq. (4) yields

$$\omega = \tan^{-1}\left\{\frac{\Delta\tau}{2G}(1-2\nu)\right\}. \tag{5}$$

Eq. (5) shows that the rotation angle ω is constant along a fault with a uniform stress drop and is independent of fault length. Thus if a fault were planar before it slips, then it will remain so after it slips provided the stress drop is uniform along the fault. Note that the fault rotates *with* the surrounding rock, not *through* it.

The rotation of a fault as a result of slip is not intuitive, but trilateration and GPS displacement data collected before and after the 1992 Landers earthquake show that it does occur (e.g. Hudnut et al., 1994). For typical earthquakes the shear stress drop along a fault is 10^1–10^2 MPa (Hanks, 1977). Assuming a host rock shear modulus of 3×10^4 MPa (Hatheway and Kiersch, 1989) and a Poisson's ratio of 0.25, Eq. (5) yields a rotation ω of approximately 10^{-4}–10^{-3} rad for a single earthquake with a uniform stress drop. The smaller rotation for Landers of about 2 μrad probably reflects in part the finite height of the fault.

3.2. Uniform stress drop along a penny-shaped fault

Westman (1965) solved for the three-dimensional displacements at the walls of a penny-shaped model fault of radius $r = a$ in an infinite elastic body. The fault-normal displacement on the fault is

$$u_y(|r| \le a, \quad y = 0) = \frac{\Delta\tau}{2G}\frac{(1-2\nu)}{2-\nu}x. \tag{6}$$

The associated rotation angle ω is:

$$\omega_{\mathrm{penny}} = \tan^{-1}\left\{\frac{\Delta\tau}{2G}\frac{(1-2\nu)}{2-\nu}\right\}. \tag{7}$$

This three-dimensional solution resembles the two-dimensional one in some key ways. The axis of rotation is in the plane of the fault, intersects the fault center, and is perpendicular to the direction of slip. The predicted rotation again is uniform. For a stress drop that is small relative to G, the terms in braces in Eqs. (5) and (7) yield the rotation angle in radians; they differ by a factor of $(2-\nu)$. The rotation amount is smaller for the penny-shaped fault, which is of finite size. The uniform rotation along a two-dimensional fault thus is a consequence of its uniform stress drop rather than its two-dimensional geometry.

4. Single faults with non-uniform stress drops

Fault strength and the stress drop accompanying fault slip are likely to be non-uniform for a variety of reasons. The rock along a fault commonly varies, as does the material within it. Substantial variations in the normal stress perpendicular to a fault (Martin and Simmons, 1993) and variations in the coefficient of friction along a fault (Cooke, 1997) cause the frictional resistance to slip to be non-uniform. Cowie and Scholz (1992b) noted that the resistance to slip might increase towards the tip of a propagating fault. Finally, deformation near the fault tip and an associated increase in resistance to slip is needed to prevent a physically implausible singularity in stresses at the fault tip (Martel, 1997). For all these reasons the stress drop during slip along a fault should vary.

The three shear strength distributions of Bürgmann et al. (1994) are examined now to see their effect on the shape of a two-dimensional fault. These are: (a) a step function; (b) a linear variation along the length of a fault; and (c) a linear increase from the fault center to the fault ends. These solutions can be combined to investigate a variety of plausible stress drop distributions. In each case the far-field shear stress parallel to the fault is held uniform. All subsequent figures compare slip distributions and fault shapes against those of the reference model.

4.1. Step function in the stress drop

Suppose that the shear stress along a fault drops to a new constant level over the interval $-a \le b < x < c \le +a$. This might occur because of uniform conditions along the fault there. Elsewhere along

the fault ($-a \le x < b$ and $c < x \le +a$) $\Delta\tau$ is zero. The expression for u_y along the fault in this case is:

$$u_y(-a \le x < b) = \frac{-\Delta\tau}{2G}(1-2\nu)\left[\frac{c-b}{2}\right], \tag{8a}$$

$$u_y(b < x < c) = \frac{\Delta\tau}{2G}(1-2\nu)\left[x - \frac{b+c}{2}\right], \tag{8b}$$

$$u_y(c < x \le a) = \frac{\Delta\tau}{2G}(1-2\nu)\left[\frac{c-b}{2}\right]. \tag{8c}$$

The right sides of Eqs. (8a) and (8c) contain only constants, whereas the right side of Eq. (8b) varies linearly with x. As Fig. 3 shows, each section of the fault trace is straight after the fault slips, but the orientations of the segments differ. The sections of the fault with no shear stress drop are displaced uniformly relative to each other and maintain their pre-slip orientation, whereas the orientation changes where the shear stress dropped ($b < x < c$). The fault is bent at $x = b$ and $x = c$. Fault-end bends have been documented (Martel, 1997), and a step in the stress drop provides an explanation for how they could occur.

Eq. (5) gives the rotation angle for the interval $b < x < c$ where the stress drop occurred, and also the difference in orientation of adjacent bent segments. Eq. (5) shows that the rotation angle depends on the stress drop, not on the length of the interval where the stress drop occurs. Note also that the straightness of a portion of a fault trace provides evidence neither for nor against a rotation or a stress drop.

The slip along the fault for this case is:

$$\Delta u_x = \frac{2\Delta\tau}{\pi G}(1-\nu)\left[(c-x)\cosh^{-1}\frac{a^2-cx}{a|x-c|} - (b-x)\cosh^{-1}\frac{a^2-bx}{a|x-b|} + \left(\sin^{-1}\frac{c}{a} - \sin^{-1}\frac{b}{a}\right)\sqrt{a^2-x^2}\right]. \tag{9}$$

As Fig. 3(b) shows, slip occurs everywhere along the fault, even where no shear stress drop occurred (see also Bürgmann et al., 1994). For a uniform shear stress drop along the fault, an elliptical slip distribution results. For a stepped stress drop distribution, the slip profile is helmet-shaped. Inflection points in the slip profile, bends in the fault, and the steps in the shear stress drop distribution all coincide (Fig. 3).

4.2. Linearly varying stress drop

In many situations the stresses along a fault might vary continuously rather than in a series of steps. Bürgmann et al. (1994) considered the possibility that the resistance to slip varied linearly from one end to another. The simplest such distribution is a linear stress drop of the form $\Delta\tau = kx/a$ where the shear stress rises on one half of the fault and drops on the other. This special case of a linear distribution would have few counterparts in nature; it yields a reversal in the sense of slip across the center of the fault. It is used here primarily for illustrative purposes.

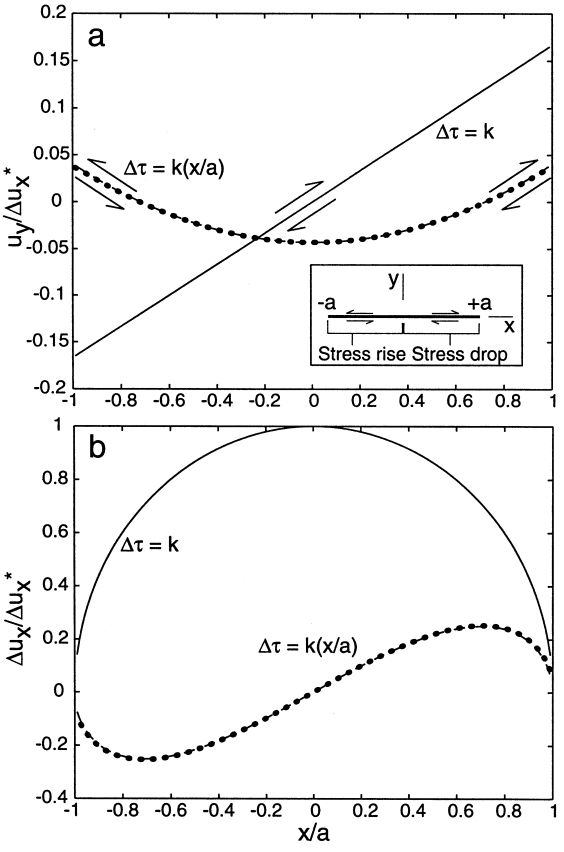

Fig. 4. Profiles of normalized (a) fault-normal displacement and (b) slip vs position (x/a) for a linear shear stress change ($\Delta\tau = kx/a$) and a constant stress drop ($\Delta\tau = k$).

For this case the fault trace geometry becomes bowed (Fig. 4a). Rotation of the fault increases towards its ends. The sign of the curvature here is constant along the fault. The shape of the fault trace is described by the equation of a parabola:

$$u_y = \frac{\Delta\tau}{4G}(1-2\nu)\left[\left(\frac{x}{a}\right)^2 - \frac{1}{2}\right]a. \tag{10a}$$

The distribution of slip is (Bürgmann et al., 1994):

$$\Delta u_x = \frac{-\Delta\tau}{G}(1-\nu)\left[\left(\frac{x}{a}\right)\sqrt{a^2-x^2}\right]. \tag{10b}$$

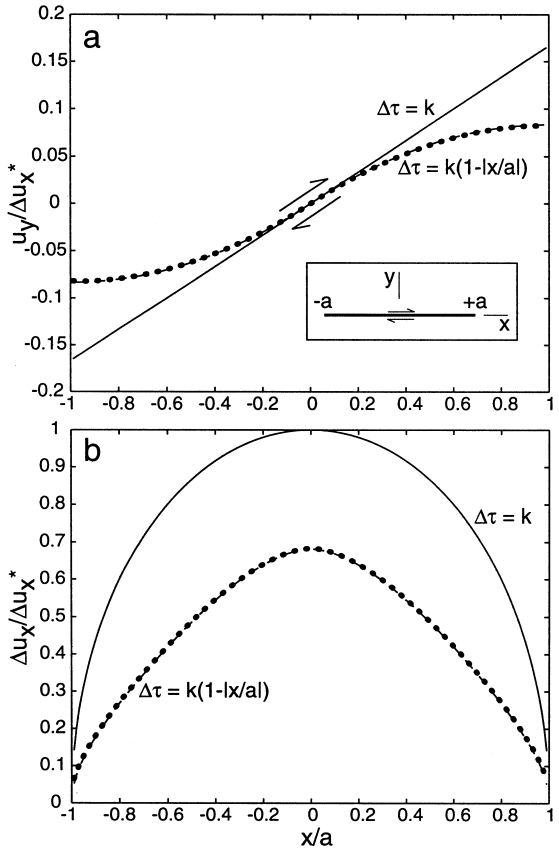

Fig. 5. Profiles of normalized (a) fault-normal displacement and (b) slip vs position (x/a) for a symmetric piecewise linear shear stress drop. The shear stress drop is $\Delta\tau = k(1 - |x/a|)$.

The sense of slip does reverse across the center of the fault (Fig. 4b).

4.3. Symmetric linear stress drop

We now consider that the resistance to slip increases linearly from the center of a fault towards its ends. This scenario is motivated in part by the work of Cowie and Scholz (1992a,b), who considered the propagation of a fault as an in-plane shear fracture. They envisioned the resistance to slip increasing towards the fault tip where the rock surrounding the fault becomes less broken and more resistant to shear failure. The stress drop is $\Delta\tau = k(1 - |x/a|)$, where the stress drop $\Delta\tau$ is a maximum at the fault center and decreases to zero at the fault ends. The sense of slip is the same along the fault. The ends of the fault will not rotate because the stress drop there is zero. Interestingly, the two halves of the fault trace again have parabolic forms (Fig. 5a) described by the following equation:

$$u_y = \frac{\Delta\tau}{2G}(1 - 2\nu)\left[\frac{x}{a}\left(1 - \frac{|x|}{2a}\right)\right]a. \tag{11a}$$

The shape of the fault trace after slip is sigmoidal, not planar, and the sign of curvature changes from one half of the fault to the other. Faults over a broad range of scale have trace geometries like this (e.g. Tchalenko and Ambraseys, 1970; Granier, 1985).

The corresponding slip along the fault is:

$$\Delta u_x = \frac{2\Delta\tau}{G}(1 - \nu)\left[\sqrt{a^2 - x^2} - \frac{1}{\pi}\left(\sqrt{a^2 - x^2} - \frac{x^2}{a}\cosh^{-1}\frac{a}{|x|}\right)\right]. \tag{11b}$$

The absolute value sign in Eq. (11b) remedies an error of Tada et al. (1973) that carried over to Eq. (14) of Bürgmann et al. (1994). The slip distribution for this theoretical case (Fig. 5b) resembles the elliptical distribution for a uniform stress drop but is more peaked.

Appendix A shows that in general the deformed geometry of an isolated, initially planar fault is directly related to the stress drop distribution. For a uniform, isotropic, isothermal host rock, if the stress drop varies as position (x/a) along a fault raised to the zero power (i.e. the stress drop is piecewise constant), then the fault-normal displacement varies as the position to the first power. The fault rotates but does not become curved. Where the stress drop varies as $(x/a)^1$ (i.e. the stress drop is piecewise linear), the fault-normal displacement varies as $(x/a)^2$. Here the fault rotates and becomes curved. As shown in Appendix A, a simple quantitative rule applies: where $\Delta\tau$ varies as $(x/a)^n$, then u_y along the fault varies as $(x/a)^{n+1}$. Appendix A also shows that the curvature of an initially planar fault provides a direct measure of the rate of change of shear stress drop along the fault.

The findings here focus on two sets of field examples. First, the faults with 'horsetail fractures' illustrated by Granier (1985) have traces that are relatively straight in the middle but that curve near their ends in the manner of Fig. 5(a). If the resistance to slip were fairly uniform near the middles of these faults, then their traces should be straight there. Theoretical considerations indicate that the resistance to slip should increase significantly near the fault ends (Martel, 1997). The curvature documented by Granier (1985) indicates that the resistance to slip increased significantly towards the fault ends in a continuous manner. If the resistance to slip had increased in a stepped manner, then the ends should be kinked rather than curved (see Martel, 1997). If the resistance to slip had diminished towards the ends, then ends should curve in the opposite sense. Second, Figs. 3(a) and 5(a) show that if the stress drop along the faults of Fig. 1 were greatest near the dike that a right-lateral kink would be produced along the left-lateral faults near the dike.

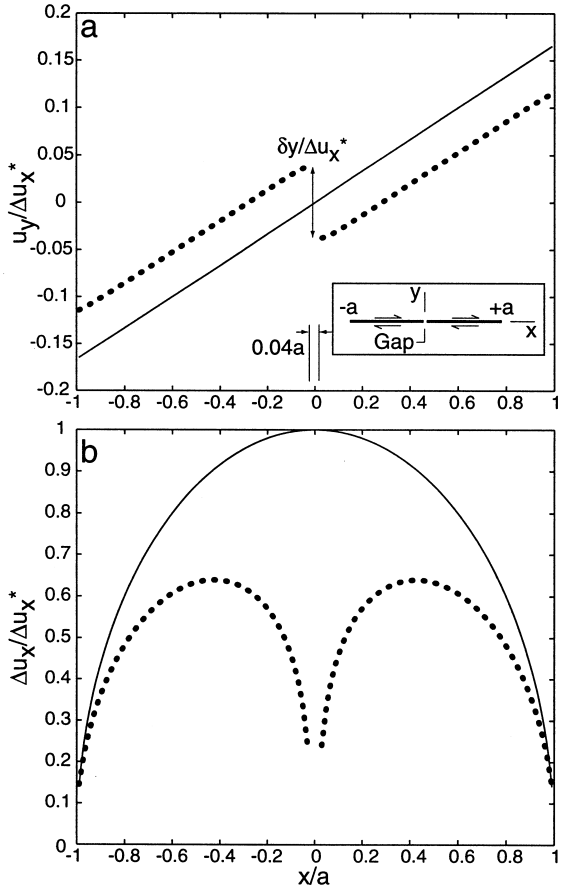

Fig. 6. Profiles of normalized (a) fault-normal displacement and (b) slip vs position (x/a) for two coplanar faults each of half-length $l = 0.99a$ separated by a gap of $0.04a$. The slip at the fault tips at $x = \pm 0.02a$ is zero.

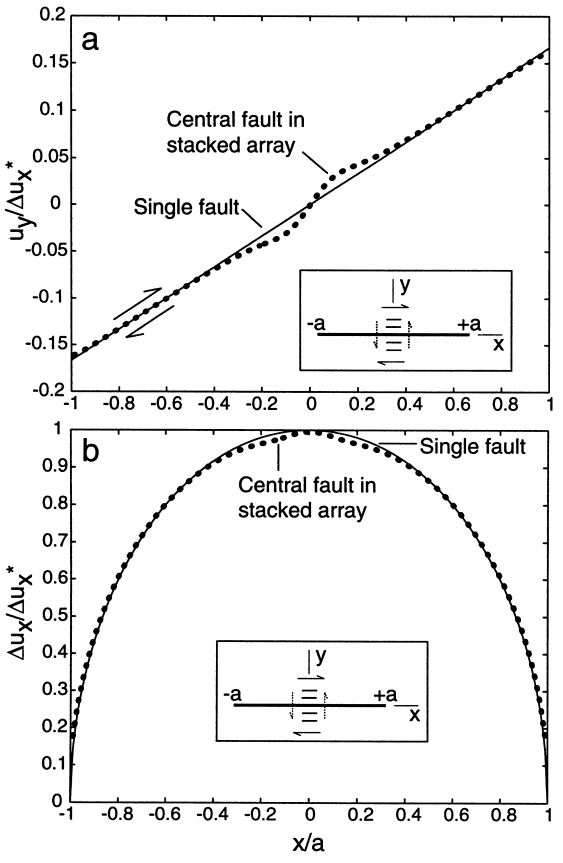

Fig. 7. Profiles of normalized (a) fault-normal displacement and (b) slip vs position (x/a) for the central fault in an array of 'stacked' faults.

5. Interaction of faults

The mechanical interaction of faults also can influence the geometry of fault arrays. Effects of fault interaction are illustrated using two examples: (1) two parallel coplanar faults (Fig. 6), and (2) a stacked array of parallel faults (Fig. 7). The former example could represent unconnected faults on opposite sides of a dike, and the latter example an array of initially unkinked faults (Fig. 1). These cases were examined using the boundary element method. In analyses of both scenarios the stress drop was taken to be uniform along the entire length of the faults.

5.1. Coplanar faults

In the analysis of coplanar faults, the length of each fault is $2l$ and the length of the two-fault array is $2a$. In Fig. 6, $l = 0.99a$. As the faults slip, both rotate in the same sense as an isolated fault (Fig. 6a). As a result, the neighboring tips of the faults rotate away from each other to yield an échelon pattern. Right-lateral slip yields a right step between the faults; left-lateral slip yields a left step. Interestingly, both options yield a dilational jog. The rotation of coplanar faults does not yield a step of the sense necessary to account for the fault geometry of Fig. 1.

A series of trials with different fault spacings show that both faults remain planar as they rotate. Furthermore, both rotate to the same orientation as a single fault that experiences the same stress drop. The relative displacement δy of the facing fault tips thus depends on the length of the individual faults but not on the original gap between them. Whereas $u_y = l(\tan \omega)$, Eq. (5) shows that

$$|\delta y| = \frac{|\Delta\tau|}{G}(1 - 2\nu)l. \tag{12}$$

For two 10 km-long faults with shear stress drops of 10 MPa, and a host rock with a shear modulus of 3×10^4 MPa and a Poisson's ratio of 0.25, δy would be 0.8 m. A pupative échelon step of this size could be produced in just one earthquake.

The slip maximum on each fault is shifted from its center towards the rock bridge between the faults (Fig. 6b). A skewed slip distribution thus arises along a

fault with a straight trace. The slip gradient is steepest near the neighboring tips, so secondary fractures would be most likely to develop there (Martel, 1997). Because a dilational jog is produced, the secondary fractures are especially likely to link the faults if they are spaced close enough. Once the faults have rotated, they could not link if they propagated in-plane.

5.2. Array of stacked faults

The model of an array of stacked faults contains five parallel faults (Fig. 7a inset). The central fault is ten times longer than the other four faults. The spacing between faults is half the length of the short faults. In the boundary element calculations, shear and normal stress drops were prescribed along the fault faces, with a unit shear stress drop and a normal stress drop of zero. These boundary conditions require the walls of the faults to slip, but they also permit the walls to open and to interpenetrate. Opening displacements are physically possible, but interpenetrations are not. To minimize interpenetration, the centers of the short faults are set along the perpendicular bisector to the long fault. Slip along the faults causes no change in the normal stress along that line and only small changes a short distance from it. The issue of interpenetration did not arise for the coplanar faults because slip causes no change in the normal stress acting across the plane of the faults.

Fig. 7(a) shows that a kink develops on the long fault, with the sense of kinking conjugate to the sense of slip. A conjugate kink arises because the central portion of the long fault rotates more than the fault as a whole. This extra rotation reflects the influence of the neighboring small faults, which rotate in the same sense as the long fault. The resulting kink is qualitatively consistent with that of Fig. 1.

The magnitude of slip along the main fault differs little from that of an isolated fault (Fig. 7b). A small decrease in slip occurs near the middle of the main fault. This reflects a sharing of slip with the neighboring small faults. The decrease in slip corresponds to a conjugate kink.

6. Effects of host rock heterogeneity

The last set of examples address how variation in Young's modulus affects the shape of a fault. Rocks show a surprisingly wide range in this elastic parameter. The values of Young's modulus tabulated by Hatheway and Kiersch (1989) range by about an order of magnitude for igneous rocks, two orders of magnitude for metamorphic rocks, and three orders of magnitude for sedimentary rocks. In keeping with the prior analyses only the displacements associated with slip are considered here.

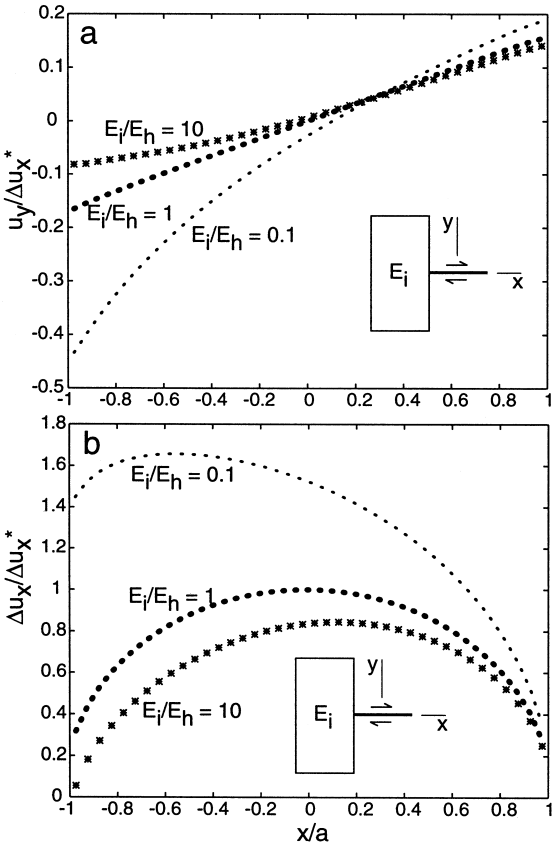

Fig. 8. Profiles of normalized (a) fault-normal displacement and (b) slip vs position (x/a) for a fault that terminates against an inclusion.

Heterogeneities in the form of the finite inclusions of Bürgmann et al. (1994) are examined here. Rectangular inclusions of different moduli are set at three positions: past a fault end (Fig. 8), along a fault end (Fig. 9), and at a fault middle (Fig. 10). The last example could represent a fault cutting through a dike (e.g. Fig. 1). The long edge of the inclusion is normal to the fault. Three different ratios of inclusion modulus to host modulus, E_i/E_h, are examined: 10:1, 1:1, and 1:10. The case of $E_i/E_h = 1$ reflects no difference in moduli and thus represents the reference case of a uniform medium. In each case Poisson's ratio of the host and the inclusion is set to 0.25. The calculations were done using a version of the boundary element code TWODD (Crouch and Starfield, 1983) modified to account for heterogeneous media. Displacements are required to be continuous across the interface between the host and the inclusion. In all cases here the shear stress drop along the fault is uniform.

Figs. 8(a), 9(a) and 10(a) show fault-normal displacement profiles. For $E_i/E_h = 1$, the u_y profile is very close to straight. The rotation of the fault is nearly uniform; small deviations reflect small artifacts in the

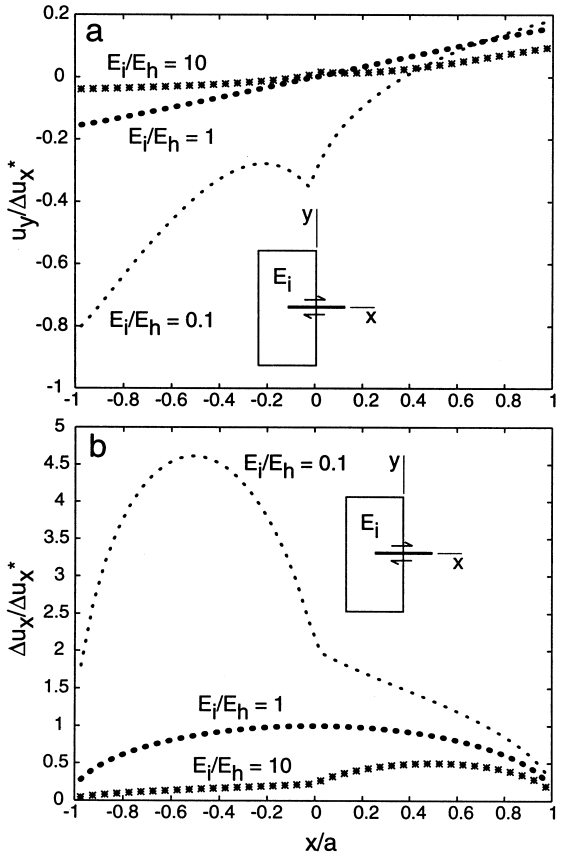

Fig. 9. Profiles of normalized (a) fault-normal displacement and (b) slip vs position (x/a) along a fault that extends into an inclusion.

numerical solution. For other ratios the profile is a complicated curve. Where the fault cuts materials of different moduli, the maximum curvature and the most complicated slip distribution occur in the more compliant material. For these examples, fault deflection tends to increase (relative to the reference case) towards a more compliant inclusion and decrease towards a more rigid inclusion. Cusps develop in the fault shape profiles at the contact between compliant and stiff materials. The sense of curvature is the same on opposite sides of the contact, but the sign of the profile slope changes. Many geologists have recognized that a fault affects its host rock; the results here show that the host rock also will affect the fault.

Figs. 8(b), 9(b) and 10(b) show the slip distributions corresponding to the respective fault-normal displacement distributions. The slip profiles here differ slightly from those of Bürgmann et al. (1994) because those analyses were conducted with a Poisson's ratio of 0 instead of 0.25. For $E_i/E_h = 1$, the slip profiles are elliptical. A stiff inclusion ($E_i/E_h = 10$) reduces the slip everywhere along the fault relative to the reference case. The slip drops most where the fault cuts the inclusion (Figs. 9b and 10b) or, if the fault does not cut the inclusion, where it approaches the inclusion (Fig. 8b). For a compliant inclusion ($E_i/E_h = 0.1$) the slip increases.

For a fault that cuts through a thin inclusion (Fig. 10a), neither a stiff nor a compliant inclusion yields a deflection profile that closely resembles the kink geometry of Fig. 1. The geometry of that kink thus is more likely to result from either a low fault strength at the dike or a stacked array of closely spaced faults rather than a modulus contrast between the dike and the host rock.

7. Discussion and conclusions

The main purpose of this paper is to show that many conditions can cause the geometry of a fault to become distorted as it slips. Conditions include variations in friction, fault strength, fault interaction, and material heterogeneity. Because these sorts of heterogeneities are inherent in the Earth, faults must deform as they slip, even for faults that were initially planar. Fault shape changes should occur on faults of all scales. On a fault of given length, shape changes will

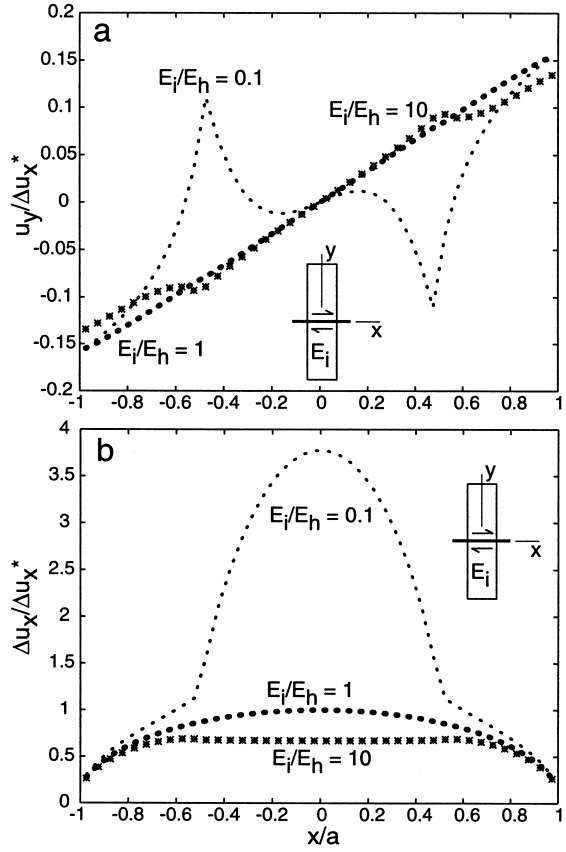

Fig. 10. Profiles of normalized (a) fault-normal displacement and (b) slip vs position (x/a) along a fault that cuts an inclusion at the fault center.

increase as slip increases. Even if a strike-slip fault were to propagate as a shear fracture, it would be unable to remain planar if the resistance to slip increased near its ends. Shape changes due to slip will occur in addition to those resulting from linkage of non-coplanar fault segments and non-uniform tectonic deformation. Although elastic effects can initiate curvature of a fault, non-elastic effects might be more important in determining its ultimate shape if they amplify the curvature.

A second key point is that fault shape can be used to illuminate the mechanics of faulting, especially if used in conjunction with data on slip distribution, fault strength, and host rock properties. Fault shape, slip distribution, and rock properties are inter-related. If two of these parameters are known, constraints can be placed on the third. Inverse techniques used to infer slip at depth along a fault (e.g. Harris and Segall, 1987) require information on fault shape and rock properties. The results here indicate that information on fault shape and slip distribution could be used to infer rock properties. Additionally, analyses of fault geometry might be useful in inferring slip along faults in homogeneous rocks on the seafloor, on other planets (e.g. Schultz, 1989), or on land where distinct markers for measuring slip are scarce.

Fig. 5 shows that grossly similar slip distributions can result for faults where the stress drop distributions are distinctly different. In contrast, a curved fault trace commonly can be distinguished from a straight one. This implies that in some cases fault shape could be analyzed more fruitfully than slip distribution to understand the stress drop distribution or strength variation along a fault. Fault shape data could also provide insight into the stress drops during slip along a fault when slip distribution data are lacking.

Fault shape and fault slip provide fundamentally different but complementary information on fault mechanics, and specifically on the stress drop during slip. In uniform isotropic rock, the slip at a point depends on the integrated effect of stress drops along the entire fault, whereas the curvature reveals details of how the stress drop varies with position along the fault. This result indicates that fault geometry is sensitive to the manner in which stresses change along a fault, perhaps more sensitive than the slip distribution is.

The theoretical findings here can be exploited by using geologic maps to relate fault shape, slip distribution, and rock types along faults. Also, fault-normal displacements identified by geodetic techniques such as GPS (Hudnut et al., 1994) or radar interferometry (Massonnet et al., 1993) could be used to investigate the variation in shear stress drop along a fault during an earthquake.

Acknowledgements

This research was supported by the U.S. Department of Energy Office of Basic Energy Sciences (Grant No. DE-FG03-85ER14525) and the Office of Naval Research (Grant No. N00014-86-1-0353). I am most grateful for this support. Reviews by Roland Bürgmann and Michele Cooke, and discussions with Garret Ito and Linda Martel contributed to a substantially improved final manuscript. This is SOEST contribution no. 4733.

Appendix A

As indicated by Eq. (1a), the fault-normal displacement along the walls of a mode II fault is proportional to value of the real component of the complex stress function $\bar{Z}$.

$$u_y = c_1 \,\mathrm{Re}\, \bar{Z}, \tag{A1}$$

where $c_1 = -(1-2\nu)/2G$. Eq. (A1) can be solved for $\mathrm{Re}\, \bar{Z}$

$$\mathrm{Re}\, \bar{Z} = \frac{u_y}{c_1}. \tag{A2}$$

The change in shear stress ($\Delta\tau$) along the walls of the fault depends on a second complex stress function Z (Tada et al., 1973; Martel, 1997):

$$\Delta\tau = \mathrm{Re}\, Z \tag{A3}$$

where Z is the derivative of $\bar{Z}$:

$$Z = \frac{\mathrm{d}\bar{Z}}{\mathrm{d}z}. \tag{A4}$$

The term z equals $x + \mathrm{i}y$. Along the walls of the fault $y = 0$, so $z = x$. Whereas $\mathrm{d}z = \mathrm{d}x$, Eqs. (A3) and (A4) yield:

$$\Delta\tau = \mathrm{Re}\frac{\mathrm{d}\bar{Z}}{\mathrm{d}x}. \tag{A5}$$

Substituting Eq. (A2) into Eq. (A5) yields a surprisingly simple relationship between $\Delta\tau$ and u_y:

$$\Delta\tau = \frac{1}{c_1}\frac{\mathrm{d}u_y}{\mathrm{d}x}. \tag{A6}$$

The shear stress drop at a point along the fault is thus proportional to the rate of change of fault-normal displacement along the fault. As a result, if u_y varies as x^{n+1}, then $\Delta\tau$ will vary as x^n. Eq. (8.34a) of Pollard and Segall (1987) reflects a special case of Eq. (A5).

The curvature magnitude K of an initially planar fault is given by the following expression (e.g. Leithold, 1976):

$$K = \frac{\left|\frac{d^2u_y}{dx^2}\right|}{\left[1+\left(\frac{du_y}{dx}\right)^2\right]^{3/2}}. \quad \text{(A7)}$$

For faults that undergo small rotations as they slip, the derivative term in the denominator of Eq. (A7) is tiny. This allows the curvature magnitude to be expressed in a simpler form:

$$K \approx \left|\frac{d^2u_y}{dx^2}\right|. \quad \text{(A8)}$$

A comparison of Eqs. (A6) and (A8) shows that the magnitude of curvature at a point along a fault is proportional to the rate of change of shear stress along the fault:

$$K \approx c_1\left|\frac{d(\Delta\tau)}{dx}\right|. \quad \text{(A9)}$$

The slip along a fault and the curvature of the fault reveal two different but related aspects of the mechanics of faulting. Eq. (1a) shows that the slip along a fault Δu_x is proportional to the imaginary part of $\bar{Z}$:

$$\Delta u_x = 2\frac{(1-\nu)}{G}\mathrm{Im}\,\bar{Z}. \quad \text{(A10)}$$

This can be recast in the following forms:

$$\Delta u_x = 2\frac{(1-\nu)}{G}\int_{-a}^{+a}\frac{d(\mathrm{Im}\,\bar{Z})}{dz}dz, \quad \text{(A11)}$$

or, using Eq. (A4), as

$$\Delta u_x = 2\frac{(1-\nu)}{G}\int_{-a}^{+a}\mathrm{Im}\,Z\,dz. \quad \text{(A12)}$$

The slip is then proportional to the integral of Z, and Eq. (A3) shows that Z is proportional to the stress drop. The slip at a point thus depends on the integral of the stress drop along the entire fault. In contrast, Eq. (A9) shows that the curvature at a point along a fault scales with the rate of change of the stress drop at that point. Simply put, fault slip reflects largely a weighted average of the stress drop, whereas fault curvature reveals how the stress drop varies spatially.

References

Aydin, A., Nur, A., 1982. Evolution of pull-apart basins and their scale independence. Tectonics 1, 91–105.

Bürgmann, R., Pollard, D.D., 1994. Strain accommodation about strike-slip fault discontinuities in granitic rock under brittle-to-ductile conditions. Journal of Structural Geology 16, 1655–1674.

Bürgmann, R., Pollard, D.D., Martel, S.J., 1994. Slip distributions on faults: effects of stress gradients, inelastic deformation, heterogeneous host-rock stiffness, and fault interaction. Journal of Structural Geology 16, 1675–1690.

Cooke, M., 1997. Fracture localization along faults with spatially varying friction. Journal of Geophysical Research 102, 22425–22434.

Cowie, P.A., Scholz, C.H., 1992a. Physical explanation for the displacement–length relationship of faults using a post-yield fracture mechanics model. Journal of Structural Geology 14, 1133–1148.

Cowie, P.A., Scholz, C.H., 1992b. Growth of faults by accumulation of seismic slip. Journal of Geophysical Research 97, 11085–11095.

Cox, S.J.D., Scholz, C.H., 1988a. An experimental study of shear fracture in rocks: mechanical observations. Journal of Geophysical Research 93, 3307–3320.

Cox, S.J.D., Scholz, C.H., 1988b. On the formation and growth of faults: an experimental study. Journal of Structural Geology 10, 413–430.

Crouch, S.L., Starfield, A.M., 1983. Boundary Element Methods in Solid Mechanics. Allen & Unwin, London.

Cruikshank, K.M., Aydin, A., 1994. Role of fracture localization in arch formation, Arches National Park, Utah. Geological Society America Bulletin 106, 879–891.

Cruikshank, K.M., Zhao, G., Johnson, A.M., 1991. Duplex structures connecting fault segments in Entrada sandstone. Journal of Structural Geology 13, 1185–1196.

Davies, R.K., Pollard, D.D., 1986. Relations between left-lateral strike-slip faults and right-lateral monoclinal kink bands in granodiorite, Mt. Abbot quadrangle, Sierra Nevada, California. Pure and Applied Geophysics 124, 177–201.

Granier, T., 1985. Origin, damping, and pattern of development of faults in granite. Tectonics 4, 721–737.

Hanks, T.C., 1977. Earthquake stress drops, ambient tectonic stress and stresses that drive plate motions. Pure and Applied Geophysics 115, 441–458.

Harris, R., Segall, P., 1987. Detection of a locked zone at depth on the Parkfield, California segment of the San Andreas fault. Journal of Geophysical Research 92, 7945–7962.

Hatheway, A.W., Kiersch, G.A., 1989. Engineering properties of rock. In: Carmichael, R.S (Ed.), Practical Handbook of Physical Properties of Rocks and Minerals. CRC Press, Boca Raton, Florida, pp. 671–715.

Hudnut, K.W., Bock, Y., Cline, M., Fang, P., Feng, Y., Freymueller, J., Ge, X., Gross, W.K., Jackson, D., Kim, M., King, N.E., Langbein, J., Larsen, S.C., Lisowski, M., Shen, Z.K., Svarc, J., Zhang, J., 1994. Co-seismic displacements of the 1992 Landers earthquake sequence. Bulletin of the Seismological Society of America 84, 625–645.

Leithold, L., 1976. The Calculus with Analytic Geometry. Harper & Row, New York.

Martel, S.J., 1990. Formation of compound strike-slip fault zones, Mount Abbot quadrangle, California. Journal of Structural Geology 12, 768–772.

Martel, S.J., 1997. Effects of cohesive zones on small faults and implications for secondary fracturing and fault trace geometry. Journal of Structural Geology 19, 835–847.

Martel, S.J., Pollard, D.D., Segall, P., 1988. Development of simple fault zones in granitic rock, Mount Abbot quadrangle, Sierra Nevada, California. Geological Society America Bulletin 100, 1451–1465.

Martin, C.D., Simmons, G.R., 1993. The Atomic Energy of Canada Limited Underground Research Laboratory; an overview of geomechanics characterization. In: Hudson, J.A (Ed.), Rock Testing and Site Characterization. Pergamon Press, Oxford, pp. 915–950.

Massonnet, D., Rossi, M., Carmona, C., Adragna, F., Peltzer, G., Feigl, K., Rabaute, T., 1993. The displacement field of the Landers earthquake mapped by radar interferometry. Nature 364, 138–142.

Petit, J.P., Barquins, M., 1988. Can natural faults propagate under mode II conditions? Tectonics 7, 1243–1256.

Pollard, D.D., Segall, P., 1987. Theoretical displacements and stresses near fractures in rock. In: Atkinson, B.K (Ed.), Fracture Mechanics of Rock. Academic Press, London, pp. 277–349.

Rispoli, R., 1981. Stress fields about strike-slip faults inferred from stylolites and tension gashes. Tectonophysics 75, T29–T36.

Scholz, C.H., Dawers, N.H., Yu, J.Z., Anders, M.H., 1993. Fault growth and fault scaling laws: preliminary results. Journal of Geophysical Research 98, 21951–21961.

Schultz, R.A., 1989. Strike-slip faulting of ridged plains near Valles Marineris, Mars. Nature 341, 424–426.

Schwartz, D.P., Coppersmith, K.J., 1986. Seismic hazards: new trends in analysis using geologic data. In: Active Tectonics. National Academy of Sciences, Washington DC, pp. 215–230.

Segall, P., Pollard, D.D., 1980. Mechanics of discontinuous faults. Journal of Geophysical Research 85, 4337–4350.

Segall, P., Pollard, D.D., 1983. Nucleation and growth of strike slip faults in granite. Journal of Geophysical Research 88, 555–568.

Sibson, R.H., 1987. Earthquake rupturing as a mineralizing agent in hydrothermal systems. Geology 15, 701–704.

Swanson, M.T., 1990. Extensional duplexing in the York Cliffs strike-slip fault system, southern coastal Maine. Journal of Structural Geology 12, 499–512.

Sylvester, A.G., 1988. Strike-slip faults. Geological Society America Bulletin 100, 1666–1703.

Tada, K., Paris, P.C., Irwin, G.R., 1973. The Stress Analysis of Cracks Handbook. Del Research Corporation, Hellertown, Pennsylvania.

Tchalenko, J.S., Ambraseys, J.S., 1970. Similarities between shear zones of different magnitudes. Geological Society America Bulletin 81, 1625–1640.

Vermilye, J.M., Scholz, C.H., 1998. The process zone: a microstructural view of fault growth. Journal of Geophysical Research 103, 12223–12237.

Wallace, R.E., Morris, H.T., 1986. Characteristics of faults and shear zones in deep mines. Pure and Applied Geophysics 124, 107–125.

Westergaard, H.M., 1939. Bearing pressures and cracks. Journal of Applied Mechanics 66, A49–A53.

Westman, R.A., 1965. Asymmetric mixed boundary value problems of the elastic half-space. Journal of Applied Mechanics 32, 411–417.

Willemse, E.J.M., Peacock, D.C.P., Aydin, A., 1997. Nucleation and growth of strike-slip faults in limestones from Somerset, U.K. Journal of Structural Geology 19, 1461–1477.

Woodcock, N.H., Fischer, M., 1986. Strike-slip duplexes. Journal of Structural Geology 8, 725–735.